

# RSC Advances



This is an *Accepted Manuscript*, which has been through the Royal Society of Chemistry peer review process and has been accepted for publication.

*Accepted Manuscripts* are published online shortly after acceptance, before technical editing, formatting and proof reading. Using this free service, authors can make their results available to the community, in citable form, before we publish the edited article. This *Accepted Manuscript* will be replaced by the edited, formatted and paginated article as soon as this is available.

You can find more information about *Accepted Manuscripts* in the [Information for Authors](#).

Please note that technical editing may introduce minor changes to the text and/or graphics, which may alter content. The journal's standard [Terms & Conditions](#) and the [Ethical guidelines](#) still apply. In no event shall the Royal Society of Chemistry be held responsible for any errors or omissions in this *Accepted Manuscript* or any consequences arising from the use of any information it contains.

## Enhanced Reproducibility of the High-Efficient Perovskite Solar-Cells via a Thermal Treatment

Yun-Jeong Kim,<sup>1</sup> Duong-Thanh Tung,<sup>2</sup> Hyung-Jin Choi,<sup>1</sup> Byeong-Ju Park,<sup>1</sup> Ji-Ho Eom,<sup>1</sup>  
Kyung-Soo Kim,<sup>3</sup> Jong-Ryul Jeong,<sup>1</sup> Soon-Gil Yoon<sup>1,\*</sup>

<sup>1</sup>Department of Materials Science and Engineering, Chungnam National University, Daeduk Science Town, 305-764, Daejeon, Korea

<sup>2</sup>Advanced Institute for Science and Technology (AIST), Hanoi University of Science and Technology (HUST), No 1, Dai Co Viet Rd., Hai Ba Trung, Hanoi, Vietnam

<sup>3</sup>Photovoltaic Lab., Korea Institute of Energy Research, 152 Gajeong-ro, Yuseong-gu, 305-343, Daejeon, Korea

\*Corresponding author: sgyoon@cnu.ac.kr

### Abstract

Thermal treatment of the cell samples after dc sputtering of the Au electrodes enhanced the reproducibility of the perovskite cell efficiencies because the thermal annealing induced the strong adhesion between each layer of the cells. The thermal annealing at 100 °C for 10 min in dry air atmosphere using the Au/HTL(hole transport layer)/dye (single-step process)/*m*-TiO<sub>2</sub>/*c*-TiO<sub>2</sub>/FTO/glass samples showed the highest efficiency of approximately  $8.57 \pm 0.26$  % with a reproducibility of the efficiency. The solar cells with perovskite dyes which were deposited and annealed in N<sub>2</sub> atmosphere using two-step process (deposition using a low and high concentrated-CH<sub>3</sub>NH<sub>3</sub>I solution) exhibited more enhanced efficiency and reproducibility ( $13.13 \pm 0.05$  %) than those ( $8.57 \pm 0.26$  %) of single-step process.

Keywords: Perovskite solar cells; Enhanced efficiency and reproducibility; Thermal treatment; Two-step process

## 1. Introduction

Material crystallinity is paramount in determining the electronic properties in the performance of electronic devices.<sup>1-4</sup> Thermal annealing is the most efficiently applied technique to increase the crystallinity of materials, especially thin films, because of its simplicity. Dye-sensitized solar cells are hybrid solar cells containing a mesostructured inorganic *n*-type oxide (TiO<sub>2</sub>) sensitized with an organic or metal complex dye, and infiltrated with an organic *p*-type hole-conductor.<sup>5</sup> Recently, the CH<sub>3</sub>NH<sub>3</sub>PbX<sub>3</sub> perovskite (X= Cl, Pb, I) with a direct band gap energy of 1.5~2 eV showed the outstanding properties as absorber layer in perovskite solar cells, which increased from 3.8% to more than 19.3% in just 4 years, and has been identified as possible base materials for high-efficiency commercial photovoltaics.<sup>6-11</sup> High power conversion efficiencies have been achieved in both mesoporous structures and planar heterojunction structure devices, using either spin-coating or thermal-evaporation deposition methods.<sup>12-15</sup>

So far, many studies have mainly focused on an efficiency enhancement of the dye-sensitized solar cells. Although the perovskite solar cells exhibited a high efficiency, average deviations of the obtained efficiencies are broad like  $\pm 0.79$ <sup>16</sup>,  $\pm 2.0$ <sup>12</sup>, and  $\pm 3.8\%$ <sup>9</sup>. These broad deviations suggested the unstability in the efficiencies of the perovskite solar cells and should be overcome for the reliable efficiency of the perovskite solar cells. The thermal annealing treatment of the perovskite solar cells was performed for the purposes such as the removal of the residual solvent from solution<sup>16</sup> and the enhancement of the crystallization.<sup>17</sup>

However, in the present study, first, thermal annealing treatment with different steps was performed for the stable interfaces of each layer. Effect of each stable layer after thermal annealing on the stable efficiency was investigated for the average efficiency deviations by

comparison with those of cells without thermal annealing. The uniformly crystallized perovskite dye is very important to enhance the efficiency because the HTL should be homogeneously deposited onto the dense perovskite dye. Second, enhanced efficiency of the perovskite solar cells was addressed using two-step process of the perovskite dye preparation, in addition to an enhanced reproducibility of solar-conversion efficiencies. Duong et al.<sup>18</sup> have presented that the two-step process which is combined by the solution technique and the vapor transport technique for the perovskite dye preparation enhanced the efficiency of the perovskite solar cells. However, two-step process in the present study addressed the modified solution technique only for simplified perovskite dye preparation, compared with the previous study<sup>18</sup>.

## 2. Experimental procedures

### 2-1) Preparation of the *compact-TiO<sub>2</sub>* (*c-TiO<sub>2</sub>*) blocking layers

For deposition of the *c-TiO<sub>2</sub>* blocking layer using nano-cluster deposition,<sup>19,20</sup> Ti(O-*i*Pr)<sub>2</sub>(*dibm*)<sub>2</sub>(Ti(O*i*-C<sub>3</sub>H<sub>7</sub>)<sub>2</sub>(C<sub>9</sub>H<sub>15</sub>-O<sub>2</sub>)<sub>2</sub>) precursors for liquid delivery process were dissolved in hexane and used as the sources of titanium at concentrations of 0.075 M. When the chemical sources entered the vaporizer, they were immediately vaporized and carried to the showerhead within the reaction chamber by the argon carrier gas at a flow rate of 100 sccm (standard cc min<sup>-1</sup>). The oxygen was supplied to the showerhead as a reaction gas at a fixed flow rate of 100 sccm. The showerhead temperature was maintained at 240–300 °C, while the substrate temperature was maintained at 400 °C for crystallization of the *c-TiO<sub>2</sub>*. The film thickness was maintained at 80 nm and its real thickness was confirmed through the cross-sectional images of the scanning electron microscopy (SEM) and transmission electron microscopy (TEM). The 600 nm thick-mesoporous TiO<sub>2</sub> (*m-TiO<sub>2</sub>*) layers were deposited onto

the TiO<sub>2</sub> blocking layer/FTO substrate via spin coating at 2,000 rpm (revolution per minute) using the TiO<sub>2</sub> paste (Dyesol 18NR-T) diluted further in methanol at ratio of 1:10, 1:7, 1:5 and 1:3 by weight. The layers were sintered in air atmosphere at 500 °C for 30 min.

### **2-2) Preparation of the perovskite dye (CH<sub>3</sub>NH<sub>3</sub>PbI<sub>3</sub>) via single-step process**

For single-step process, CH<sub>3</sub>NH<sub>3</sub>I was synthesized by reacting the 24 mL of methylamine (33 wt % in absolute ethanol, Sigma) and 10 mL of hydroiodic acid (57 wt % in water, Aldrich) in a 250 mL round-bottom flask at 0 °C for 2 h with stirring. The precipitate was recovered by putting the solution on a rotary evaporator and carefully removing the solvents at 50 °C. The raw product CH<sub>3</sub>NH<sub>3</sub>I was re-dissolved in 80 mL absolute ethanol and precipitated with the addition of 300 mL diethyl ether. After filtration, the step was repeated again, and the solid was collected and dried at 60 °C in a vacuum oven for 24 h. Then, 1.157 g of PbI<sub>2</sub> and 0.395 g of CH<sub>3</sub>NH<sub>3</sub>I were dissolved in 2.0 mL  $\gamma$ -butyrolactone solution at 60 °C. The clear perovskite precursor solution was first spread on the *m*-TiO<sub>2</sub> films for 5 s and then was spun at 4,000 rpm for 30 s in air atmosphere. The deposited CH<sub>3</sub>NH<sub>3</sub>PbI<sub>3</sub> films were finally dried on a hot-plate at 100 °C for 10 min.

### **2-3) Preparation of the perovskite dye via two-step process**

For two-step process, PbI<sub>2</sub> solution was spin-coated at 4,000 rpm for 40 s onto the 200 nm-thick *m*-TiO<sub>2</sub> layers. The PbI<sub>2</sub> solution was prepared at 60 °C using PbI<sub>2</sub> (0.04g) and DMF (~ ml). The PbI<sub>2</sub> was coated onto the *m*-TiO<sub>2</sub> layers by a flowing the hot air to maintain at 60 °C which is the temperature of the substrate during the deposition. If the substrate temperature for the deposition of PbI<sub>2</sub> is lower than temperature of the PbI<sub>2</sub> solution, the deposited PbI<sub>2</sub> becomes to be opaque. Although the deposited PbI<sub>2</sub> is transparent by a flow of a hot air during the deposition, the PbI<sub>2</sub> does not penetrate into the thicker *m*-TiO<sub>2</sub> layer because the

solvent of the  $\text{PbI}_2$  solution is rapidly evaporated. Therefore, thickness of the  $m\text{-TiO}_2$  layer in the case of a two-step process should be reduced rather than that in the single-step process.

A low concentrated- $\text{CH}_3\text{NH}_3\text{I}$  solution (2 mg/1 ml) was spin-coated at 2,000 rpm for 5 s onto the  $\text{PbI}_2$ -coated  $m\text{-TiO}_2$  layers and then high concentrated- $\text{CH}_3\text{NH}_3\text{I}$  solution (40 mg/1 ml) was dropped onto the low-concentrated  $\text{CH}_3\text{NH}_3\text{I}$  layer and was maintained for 3-4 minutes for stable wetting with the low-concentrated  $\text{CH}_3\text{NH}_3\text{I}$  layer. The sample was maintained at 2,000 rpm for 20 s. After spin-coating of the low and high-concentrated  $\text{CH}_3\text{NH}_3\text{I}$  layer, samples were annealed for various duration times under dry air and  $\text{N}_2$  atmosphere at 100 °C.

#### **2-4) Preparation of the HTL and Au top electrode**

A HTL was prepared on the  $\text{FTO}/c\text{-TiO}_2/m\text{-TiO}_2/\text{perovskite}$  dye substrate by spin coating (at 2,500 rpm for 40 s) using a hole transport solution (HTM), where a spiro-OMeTAD (Lumtec)/chlorobenzene (180 mg/1 mL) solution was employed with addition of 50  $\mu\text{L}$  Libis( trifluoromethanesulfonyl) imide (Li-TFSI, Sigma)/acetonitrile (170 mg/1mL) and 20  $\mu\text{L}$  tert-butylpyridine (tBP, Sigma). Finally, the 80 nm-thick Au films as a counter electrode was deposited by dc (direct current) sputtering under a working pressure of 0.4 Pa (base pressure of  $6.6 \times 10^{-3}$  Pa) using a gold target of 2 inch diameter. The active area of the cell was approximately  $0.25 \text{ cm}^2$ .

#### **2-5) Characterization of the perovskite solar cells**

The cross-sectional images of  $c\text{-TiO}_2$ ,  $m\text{-TiO}_2$ , and perovskite dye were analyzed using SEM (TOPCON DS-130C). The crystalline structure and the preferred orientation of the  $c\text{-TiO}_2$  and the perovskite dye films were characterized by X-ray diffraction (XRD, Rigaku D/MAX-RC) using  $\text{Cu } K\alpha$  radiation and a nickel filter. Photocurrent–voltage (I-V)

characteristics of the solar cells were measured using an IVIUMSTAT under illumination from a Sun 3000 solar simulator composed of 1,000 W mercury-based Xe arc lamps and AM 1.5-G filters. Light intensity was calibrated with a silicon photodiode. For stability of the each layer, Au/HTL/Dye/*m*-TiO<sub>2</sub>/*c*-TiO<sub>2</sub>/FTO/glass samples were thermally annealed both at different temperatures for 10 min and for different times at 100 °C via rapid-thermal annealing (RTA) under a dry air atmosphere. The increasing rate of the temperature in RTA process was approximately 8.3 °C/s.

### 3. Results and discussion

#### 3-1) Enhanced reproducibility of the solar cells with perovskite dyes prepared via single-step process

Effect of thermal treatment on the reproducibility of the absolute photo-conversion efficiency was investigated using Au/HTL/perovskite dye/*m*-TiO<sub>2</sub>/*c*-TiO<sub>2</sub>/FTO/glass. Figure 1 (a) shows variations in current density vs. voltage measured using different annealed samples. The red colors in an inset of Fig. 1(a) showed the samples annealed at different processes. The perovskite dye in all of samples was annealed at 100 °C for 10 min in dry air atmosphere for crystallization. The thermal treatment of the samples was performed under the same conditions (at 100 °C for 10 min under dry air atmosphere) after deposition at each step of dye, HTL, and Au electrode. For example, in the thermal treatment process of sample “3”, dye/(*m/c*)-TiO<sub>2</sub>/FTO structure was annealed at 100 °C for 10 min under air atmosphere and then Au top electrode/HTL/dye/(*m/c*)-TiO<sub>2</sub>/FTO structure was annealed at the same condition again. The thermal treatment for the crystallization of the perovskite dye was only performed in the most of researches reported already, as shown in sample “4”. Sample “4” showed a low current density of around 15.7 mA cm<sup>-2</sup> and a low open circuit voltage ( $V_{OC}$ ) of

approximately 0.62 V. Especially, sample “4” showed a large deviation ( $\pm 1.04$ ) of the efficiency. However, for stability of an interface between each layer, thermal treatment of each layer under the same conditions, as shown in sample “2”, showed the lowest current density of approximately  $6.38 \text{ mA cm}^{-2}$  and a  $V_{OC}$  of around 0.69 V. The photovoltaic performances of the samples annealed at each layer were summarized at Table 1. As shown in Fig. 1(a), thermal annealing of both perovskite dye and Au electrode layers, as shown in the case of sample “3”, showed the highest current density of approximately  $21.6 \text{ mA cm}^{-2}$  and an open circuit voltage of 0.8 V. The photo-conversion efficiency of the sample “3” was approximately  $8.57 \pm 0.26 \%$ , indicating a low deviation of efficiency, as compared with those reported previously without the thermal treatment. In the present study, for effective thermal effect of the perovskite solar cells, Au electrodes deposited onto the HTL were thermally annealed both for different times at  $100 \text{ }^\circ\text{C}$  and at different temperatures for 10 min. Figure 1(b) shows the relationship between current density and voltage of the samples annealed at  $100 \text{ }^\circ\text{C}$  for different times. The current density of the perovskite cells increased as annealing time increases from 5 to 10 min, while an increase of annealing time above 10 min induced the decrease of current density. The HTL is sensitive to the temperature and atmosphere during the thermal treatment. The charge-transport studies of the HTL treated under an air atmosphere revealed the incorporation of gas molecules causing a decrease in charge mobility.<sup>21</sup> Therefore, annealing for a long time above 10 min at  $100 \text{ }^\circ\text{C}$  under air atmosphere decreased the efficiencies of the perovskite solar cells by a deteriorated HTL.

The photovoltaic properties of the perovskite cells annealed for different times at  $100 \text{ }^\circ\text{C}$  were summarized at Table 2. Based on the photovoltaic performance annealed for different times, although the thermal treatment is required for enhancement of the properties,

appropriate optimum conditions for annealing time were observed at an annealing temperature of 100 °C. The effect of annealing temperature on the photovoltaic performance was shown in Fig. 1(c) for annealing time of 10 min. Both the current density and the open circuit voltage of the cells increased with increasing annealing temperature from 80 to 100 °C, while both properties decreased with increasing temperature above 100 °C. The photovoltaic properties of the solar cells as a function of annealing temperature for annealing time of 10 min were summarized at Table 3. Based on the photovoltaic performances of the thermally treated perovskite cells, optimum conditions were observed at 100 °C for 10 min in dry air atmosphere after Au deposition by dc sputtering. However, the small deviations of the absolute photo-conversion efficiency were observed at all of thermally treated conditions. This result absolutely suggested that the thermal treatment was required for a stable efficiency of the perovskite cells.

The crystallinity and the morphologies of the perovskite cells were characterized using XRD and SEM cross-sectional images and they were shown in Figs. 2(a) and 2(b), respectively. The XRD patterns before and after annealing at 100 °C for 10 min in air atmosphere were measured using the HTL/perovskite dye/meso-TiO<sub>2</sub>/c-TiO<sub>2</sub>/FTO/glass samples. Here, before and after annealed samples meant the sample “4” and sample “3”, respectively, as shown in an inset of Fig. 1(a). Based on the XRD patterns of the samples, samples before and after annealing showed the crystallized peaks that were attributed to the *m*-TiO<sub>2</sub> and perovskite dye. The peak intensities of the crystalline phases after annealing were not remarkably changed because they were annealed at a low temperature of 100 °C, as compared with those before annealing. The morphologies of the Au/HTL/perovskite dye/*m*-TiO<sub>2</sub>/c-TiO<sub>2</sub>/FTO/glass samples before and after annealing were investigated using SEM

cross-sectional images and the images were shown in Figs. 2 (b) and 2 (c), respectively. Based on the SEM cross-sectional images, each layer was clearly shown without both morphology and thickness change by the thermal treatment. However, typical site at the interface between Au and HTL shown in Fig. 2(b) was enlarged and it was shown in Fig. 2(b-1). The *in situ* dc sputtered Au electrode onto the HTL without an Au electrode annealing showed a weak adhesion with a HTL. On the other hand, Au electrode annealed at 100 °C for 10 min in a dry air atmosphere showed a strong adhesion with a HTL, as shown in Fig. 2 (c-1). Based on the adhesion property between dc sputtered Au electrode and HTL, the reproducible efficiency is dominantly dependent on the adhesion of the Au top electrode with the HTL.

The internal resistances of the perovskite cells before (sample “4”) and after (sample “3”) annealing were studied via electrochemical impedance spectroscopy (EIS) at frequencies that ranged from 0.1 Hz to 100 kHz, and alternating current amplitude of 10 mV. Figure 3 (a) shows the EIS results at forward bias of the open-circuit voltage under light irradiation of 100 mW cm<sup>-2</sup>, and the results are represented as Nyquist plots. The full cells measured before and after annealing showed two different semicircles with different resistances, which were fitted by the equivalent circuit shown in the inset of Fig. 3(a) using Z-view software.<sup>20</sup> The structure of the full cells was Au electrode/HTL/Absorber layer/(*m/c*)-TiO<sub>2</sub> layer/FTO. Here, number ①, ②, and ③ indicated the resistance of the FTO, interface resistance between Au and HTL, and the mixed interface resistances of *m*-TiO<sub>2</sub>/dye and dye/HTLs, respectively. The first (sample ②’) and second (sample ③’) semicircles of the perovskite solar cells after annealing were smaller than those of the cells before annealing, which indicated the enhanced interfacial adhesion between each layer by a thermal treatment. Based on the EIS results, the

optimized thermal treatment can induce the reliable efficiency of the perovskite solar cell. Figure 3(b) shows the incident-photon-to-current-conversion efficiency (IPCE) of the perovskite solar cells before and after annealing. The IPCEs were increased by a thermal treatment when they were compared with that of before annealing. The increase in IPCEs was consistent with the increase in the  $J_{SC}$ , as shown in Figs. 1 (b) and 1(c). The IPCE values of the annealed perovskite cells showed an increase of about 12 %, compared with those of before annealed samples at a peak wavelength of 460 nm. The IPCE curves of the before and after annealed samples showed similar values at shorter wavelength ranges of 300 to 450 nm. However, the difference was large at wavelength ranges of 450 to 750 nm. The IPCE curves as a function of wavelength in both samples are dependent on the state of the absorber layer. At the long wavelength of 450-750 nm, driving force of the carriers is low. The interface states of the annealed samples were improved by a thermal treatment. Therefore, transport of the carriers in annealed samples is easier than that of the before annealed samples although the driving force for the transport of the carriers is low. As a result, the difference between IPCE curves of the before and after annealed samples becomes to be high at a wavelength of 450-750 nm. Effect of the adhesion properties of the interfacial layers on the photovoltaic properties was confirmed by a photovoltage transient study. Figure 3 (c) shows the decay of the open-circuit voltage ( $V_{OC}$ ) of the perovskite cells before and after annealing. The  $V_{OC}$  decayed rapidly for as-deposited samples after illumination was interrupted, while it decayed only slightly for the annealed samples. The slower decay of  $V_{oc}$  in annealed samples indicates slower recombination rate and longer lifetime of carriers, indicating a better cell performance.

### **3-2) Enhanced efficiency and reproducibility of the solar cells with perovskite dyes prepared via two-step process**

For enhancement of the cell efficiencies in addition to the enhancement of the reproducibility, two-step process for perovskite dye deposition were addressed under different annealing times at 100 °C. Although the perovskite solar cells without the *m*-TiO<sub>2</sub> layer have been reported to present a high efficiency of approximately 11.4 %, <sup>22</sup> 200 nm-thick *m*-TiO<sub>2</sub> layer in the present study was used for enhancement of the efficiency as well as a high reproducibility. Figure 4 showed SEM surface images of the perovskite dyes annealed for (a) 30, (b) 60, and (c) 120 min at 100 °C in dry air atmosphere. The deposition of the perovskite dye using two-step process was performed in air atmosphere at room temperature. The annealing process was performed under dry air atmosphere in tube furnace after evacuation. Samples annealed for 60 min showed denser and more homogeneous structures than those annealed for 30 min. On the other hand, samples annealed for 120 min showed large grains having nonhomogeneous grain size distributions. Samples were composed of the large and small grains. In order to improve the grain size distribution, two-step process for perovskite deposition were performed under N<sub>2</sub> atmosphere to prevent the penetration of the humidity. After deposition of the perovskite dye, annealing treatment of the dye was also performed under N<sub>2</sub> atmosphere. Figure 4 (d) showed the SEM surface image of the perovskite dye annealed for 120 min at 100 °C in N<sub>2</sub> atmosphere. Samples showed the homogeneous distributions, indicating the large grains with mean size of approximately 1.5 μm. During the preparation of the dye, humidity in air atmosphere was penetrated into the dye and it hindered the uniform growth of the grains, resulting in nonhomogeneous grain growth of the dye. Figure 4 (e) showed the SEM cross-sectional image of the devices involving a perovskite dye prepared in N<sub>2</sub> atmosphere. Based on the cross-sectional image, each layer was clearly observed as shown in figure. Each layer was approximately 200 nm-thick *m*-TiO<sub>2</sub>, 300 nm-

thick  $\text{CH}_3\text{NH}_3\text{PbI}_3$ , 200 nm-thick HTM, and 80 nm-thick Au electrodes.

Figure 5 showed the photovoltaic properties of the perovskite solar cells with perovskite dyes annealed for 30, 60, and 120 min in dry air atmosphere at 100 °C. Compared with the photovoltaic properties of the cells with perovskite dyes prepared by single-step process (Fig. 1), the solar cells with perovskite dyes prepared by two-step process showed a high open-circuit voltage ( $V_{OC}$ ) of approximately 1.02-1.04 V. This result suggested that the homogeneous morphologies of the perovskite dye played an important role in an increase of the open-circuit voltage of the cells. The photo-conversion efficiencies of the cells with perovskite dyes annealed at 30, 60, and 120 min were approximately  $10.62 \pm 0.03$ ,  $11.35 \pm 0.04$ , and  $11.96 \pm 0.03$ , respectively. The efficiencies using two-step process showed an increase of about 28%, as compared with those of samples prepared using single-step process. The  $I$ - $V$  curve of the cells with a perovskite dye prepared by two-step process onto the 600 nm-thick  $m$ - $\text{TiO}_2$  layers was shown in Fig. 1S (supplementary information). As shown in Fig. 1S, all of  $J_{sc}$ ,  $V_{oc}$ , and  $FF$  were reduced, as compared with samples prepared by two-step process onto the 200 nm-thick  $m$ - $\text{TiO}_2$  layers. In the case of a single-step process deposited onto the 600 nm-thick  $m$ - $\text{TiO}_2$  layers, because the perovskite dye of the  $\text{CH}_3\text{NH}_3\text{PbI}_2$  was completely diffused into the thicker  $m$ - $\text{TiO}_2$  layers, the remarkable efficiency was observed. However, in the case of two-step process, because the complete infiltration of the  $\text{PbI}_2$  into the  $m$ - $\text{TiO}_2$  layers is difficult if the  $m$ - $\text{TiO}_2$  layer is too thick, thickness of  $m$ - $\text{TiO}_2$  layer was reduced to 200 nm, compared with those used by a single-step process. Especially, the reproducibility of the efficiencies using two-step process was remarkably enhanced rather than that of the efficiencies using single-step process. The  $J$ - $V$  relationship of the cells with perovskite dye performed in  $\text{N}_2$  atmosphere both annealing and the deposition by two-step

process was shown in Fig. 6. Compared with the results of Fig. 5, fill factor (FF) of the cells with perovskite dye performed in N<sub>2</sub> atmosphere was enhanced rather than the cells with perovskite dye performed in air atmosphere. This result suggested that the fill factor of the perovskite solar cells was influenced by humidity in air atmosphere. The perovskite solar cells with perovskite dyes performed in N<sub>2</sub> atmosphere exhibited short-current density of 21.4 mA cm<sup>-2</sup>, open-circuit voltage of 1.04 V, fill factor of 59 %, and conversion efficiency of 13.13 ± 0.05 %. The solar cells with perovskite dyes prepared using two-step process showed more enhanced efficiency and reproducibility than those of single-step process.

#### 4. Conclusions

Thermal treatment of the cell samples after dc sputtering of the Au electrodes enhanced the reproducibility of the perovskite cell efficiencies because the thermal annealing induced the strong adhesion between each layer of the cells. The thermal annealing at 100 °C for 10 min in dry air atmosphere using the Au/HTL/dye (single-step process)/m-TiO<sub>2</sub>/c-TiO<sub>2</sub>/FTO/glass samples showed the highest efficiency of approximately 8.57 ± 0.26 % with a reproducibility of the efficiency. For enhanced efficiency and reproducibility, perovskite dyes were prepared using two-step process. The perovskite solar cells with perovskite dyes which were prepared using two-step process, deposited and annealed in N<sub>2</sub> atmosphere exhibited short-current density of 21.4 mA cm<sup>-2</sup>, open-circuit voltage of 1.04 V, fill factor of 59 %, and conversion efficiency of 13.13 ± 0.05 %.

#### *Acknowledgement*

This work was supported by the National Research Foundation of Korea (NRF) grant funded by the Korea government (MSIP) (No. NRF-2013R1A4A1069528).

## References

1. G. Li, V. Shrotriya, J. Huang, Y. Yao, T. Moriarty, K. Emery, Y. Yang, *Nat. Mater.* 2005, **4**, 864.
2. X. Liu, H. Wang, T. Yang, W. Zhang, X. Gong, *ACS Appl. Mater. Interfaces* 2012, **4**, 3701.
3. G. Li, Y. Yao, H. Yang, V. Shrotriya, G. Yang, Y. Yang, *Adv. Funct. Mater.* 2007, **17**, 1636.
4. Q. Chen, H. Zhou, Z. Hong, S. Luo, H. –S. Duan, H. –H. Wang, Y. Liu, G. Li, Y. Yang, *J. Am. Chem. Soc.* 2013, **136**, 622.
5. B. O'Regan and M. A. Grätzel, *Nature* 1991, **353**, 737.
6. A. Kojima, K. Teshima, Y. Shirai, T. Miyasaka, *J. Am. Chem. Soc.* 2009, **131**, 6050.
7. M. Lee, J. Teuscher, T. Miyasaka, T. Murakami, H. Snaith, *Science*, 2012, **338**, 643.
8. H. J. Snaith, *J. Phys. Chem. Lett.* 2013, **4**, 3623.
9. N. J. Jeon, J. Noh, Y. Kim, W. Yang, J. Seo, and S. Seok, *Nat. Mater.*, 2014, **13**, 897.
10. R. Service, *Science*, 2014, **344**, 485, 6183.
11. J. Noh, S. Im, J. Heo, T. Mandal and S. I. Seok, *Nano Lett.* 2013, **13**, 1764.
12. M. Liu, M. B. Johnston, H. J. Snaith, *Nature* 2013, **501**, 395.
13. A. Kojima, K. Teshima, Y. Shirai, T. Miyasaka, *J. Am. Chem. Soc.* 2009, **131**, 6050.
14. J. H. Heo, S. H. Im, J. H. Noh, T. N. Mandal, C. –S. Lim, J. A. Chang, Y. H. Lee, H. –J. Kim, A. Sarkar, M. K. Nazeeruddin, *Nat. Photonics* 2013, **7**, 486.

15. P. Docampo, J. M. Ball, M. Darwich, G. E. Eperon, H. J. Snaith, *Nat. Commun.* 2013, **4**, 2761.
16. Z. Xiao, Q. Dong, C. Bi, Y. Shao, Y. Yuan, and J. Huang, *Adv. Mater.* 2014, **26**, 6503.
17. H. L. Hsu, C. P. Chen, J. Y. Chang, Y. Y. Yu, and Y. K. Shen, *Nanoscale*, 2014, **6**, 10281.
18. T. T. Duong, Y. J. Kim, J. H. Eom, J. S. Choi, A. T. Le, and S. G. Yoon, *RSC Advances*, 2015, **5**, 33515.
19. T. T. Duong, H. J. Choi, S. G. Yoon, *J. Alloy. Compd.* 2014, **591**, 1.
20. T. T. Duong, H. J. Choi, Q. J. He, A. T. Le, S. G. Yoon, *J. Alloy. Compd.* 2013, **561**, 206.
21. L. K. Ono, P. Schulz, J. J. Endres, G. O. Nikiforov, Y. Kato, A. Kahn, and Y. Qi, *J. Phys. Chem. Lett.* 2014, **5**, 1374.
22. G. E. Eperon, V. M. Burlakov, P. Docampo, A. Goriely, and H. J. Snaith, *Adv. Funct. Mater.* 2014, **24**, 151.

**Figure captions**

- Fig. 1 (a) Relationship between current density and voltage measured using samples annealed at different processes. Inset of Fig. 1(a) showed various annealed processes. Red colors in inset indicated the thermally treated process. Variations in current density vs. voltage measured using perovskite cells annealed (b) at 100 °C for different times and (c) at different temperatures for 10 min in a dry air atmosphere.
- Fig. 2 (a) XRD patterns before and after annealing at 100 °C for 10 min in air atmosphere using Au/HTL/perovskite dye/*m*-TiO<sub>2</sub>/*c*-TiO<sub>2</sub>/FTO/glass samples. Here, XRD patterns of the Au top electrode were removed. (b) and (c) SEM cross-sectional image of Au/HTL/perovskite dye/*m*-TiO<sub>2</sub>/*c*-TiO<sub>2</sub>/FTO/glass samples measured before and after annealing at 100 °C for 10 min in air atmosphere, respectively. (b-1) and (c-1) Enlarged SEM cross-sectional image observed at optional places of an interfacial layer between Au and HTL from (b) and (c), respectively.
- Fig. 3 (a) Nyquist plots of the perovskite cells before and after annealing at 100 °C for 10 min in air atmosphere. The inset shows the equivalent circuit. (b) Incident-photon-to-current-conversion efficiency (IPCE) of the perovskite solar cells before and after annealing, and (c) Decay of the open-circuit voltage ( $V_{OC}$ ) of the perovskite cells before and after annealing.
- Fig. 4 SEM surface images of the perovskite dyes, which were prepared by two-step process, annealed for (a) 30, (b) 60, (c) 120 min at 100 °C in dry air atmosphere, and (d) 120 min at 100 °C in N<sub>2</sub> atmosphere. (e) SEM cross-sectional image of the

devices with a perovskite dye prepared in N<sub>2</sub> atmosphere.

Fig. 5 Photovoltaic properties of the perovskite solar cells with perovskite dyes annealed for 30, 60, and 120 min in dry air atmosphere at 100 °C. Inset showed the photovoltaic parameters of the cells with perovskite dyes annealed for different duration times in dry air atmosphere at 100 °C.

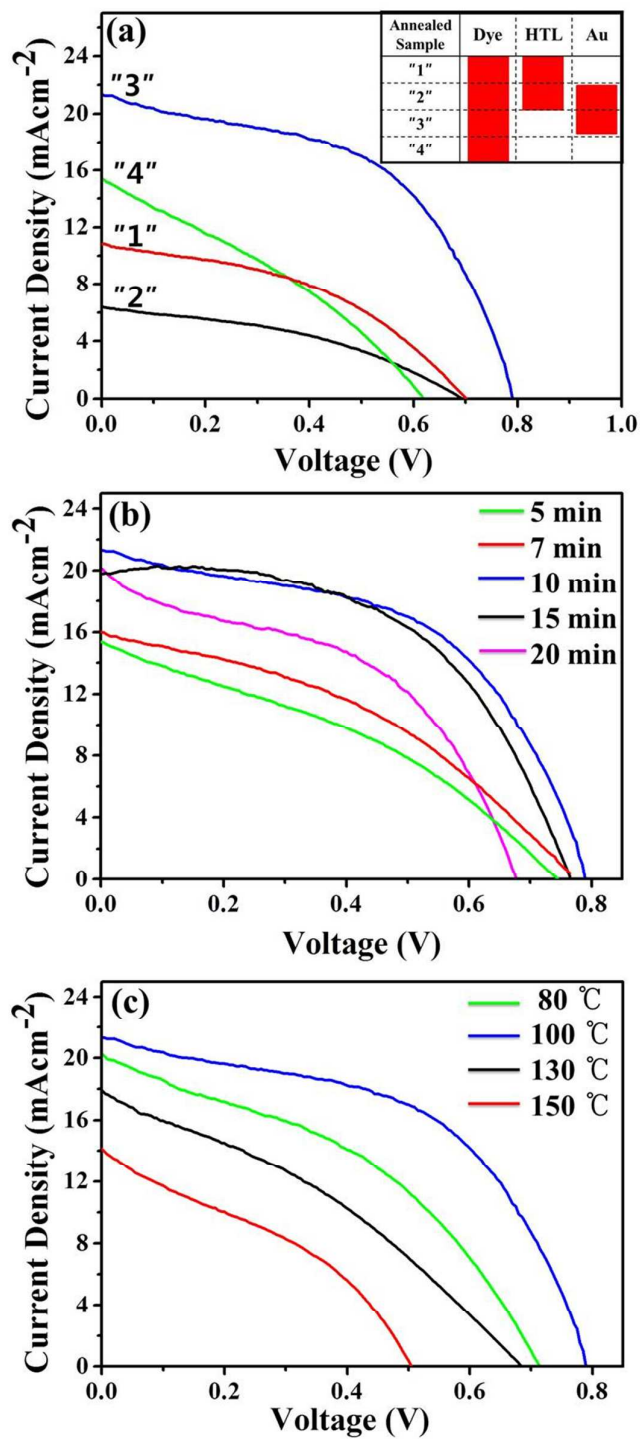
Fig. 6 Photovoltaic properties of the perovskite solar cells with perovskite dyes annealed for 120 min in N<sub>2</sub> atmosphere at 100 °C. Inset showed the photovoltaic parameters of the cells with perovskite dyes annealed for 120 min in N<sub>2</sub> atmosphere at 100 °C.

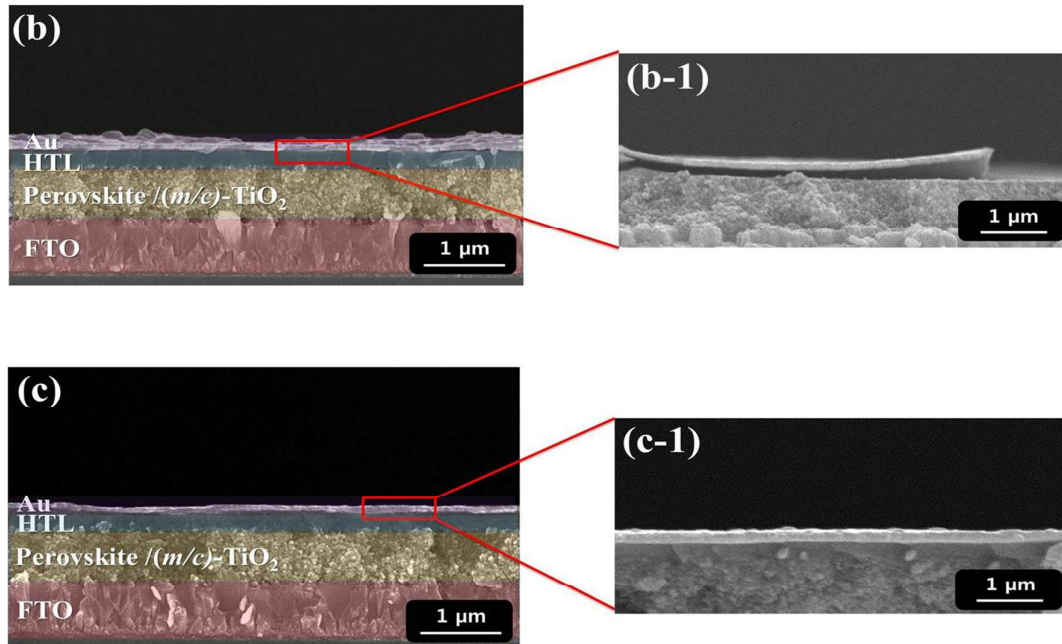
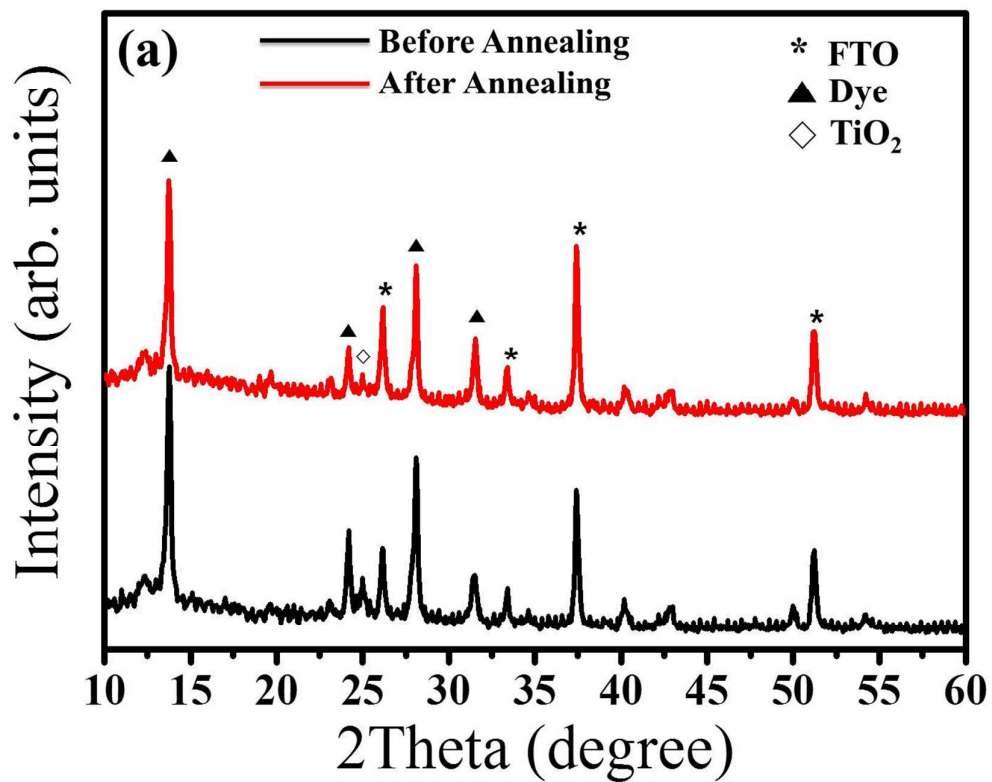
#### Table Captions

**Table 1** The photovoltaic performances of the samples annealed at each layer. The perovskite dyes were prepared using single-step process.

**Table 2** The photovoltaic properties of the perovskite cells annealed for different times at 100 °C. The perovskite dyes were prepared using single-step process.

**Table 3** The photovoltaic properties of the solar cells as a function of annealing temperature for annealing time of 10 min. The perovskite dyes were prepared using single-step process.

**Fig. 1***Y. J. Kim et. al*

**Fig. 2***Y. J. Kim et. al*

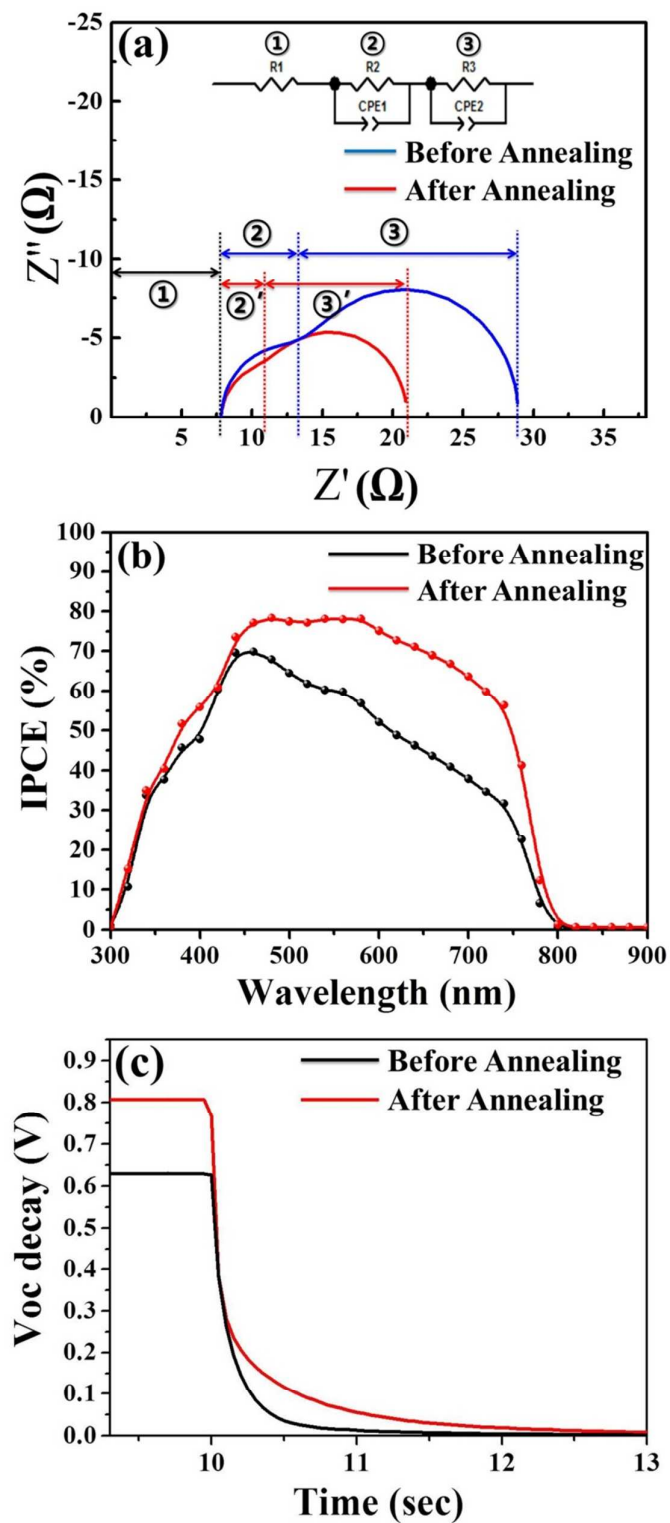
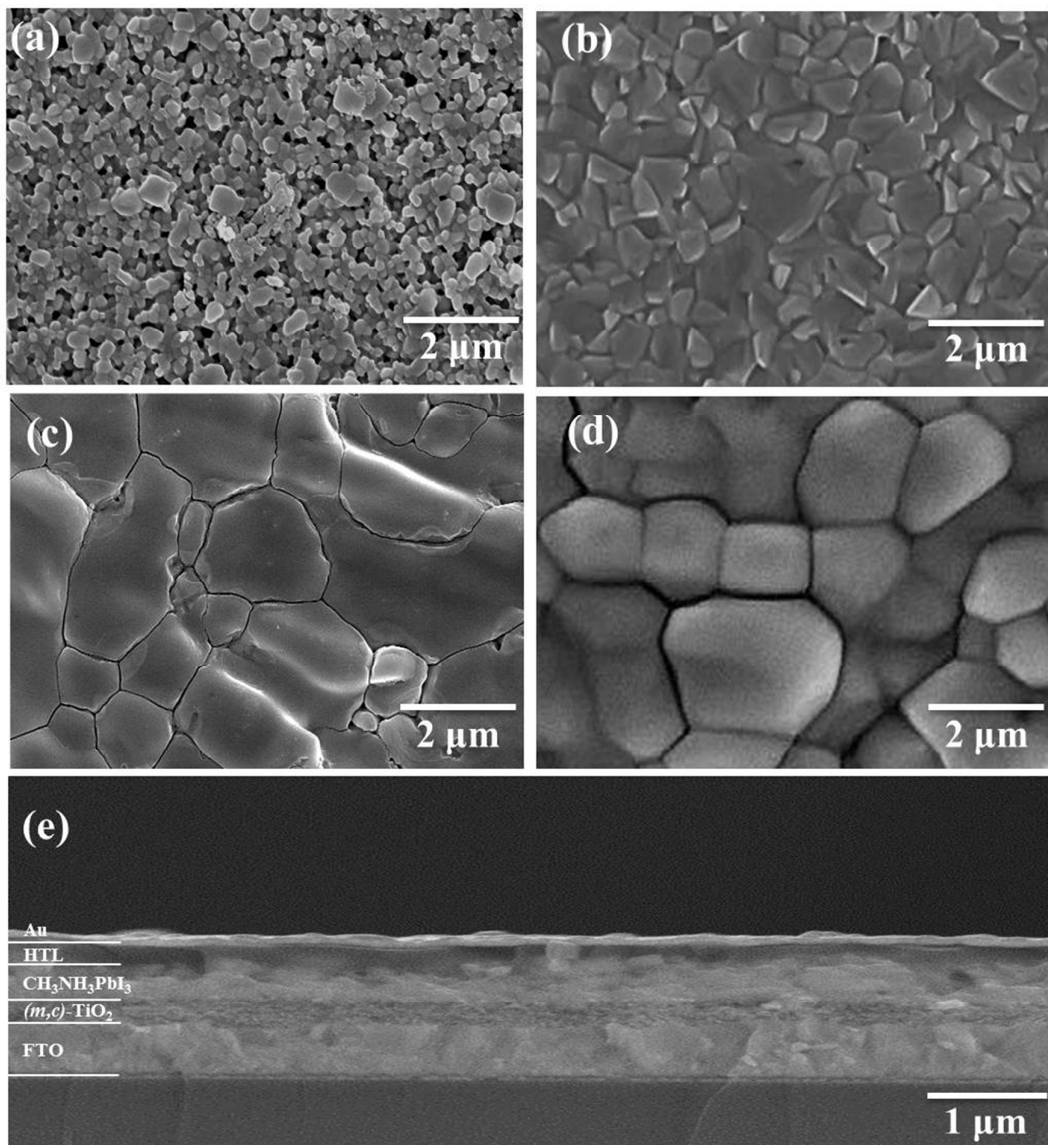
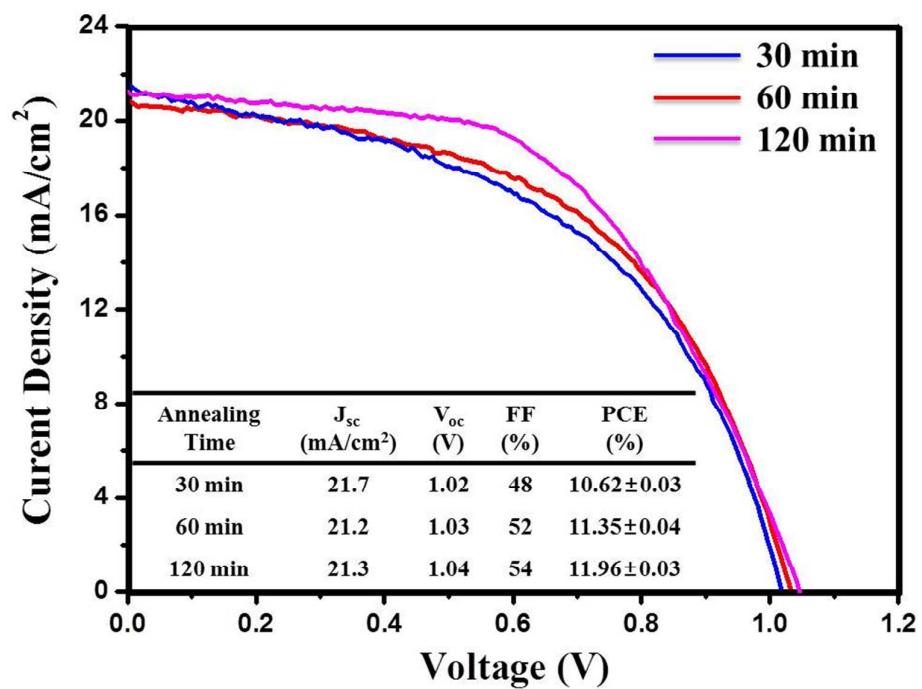
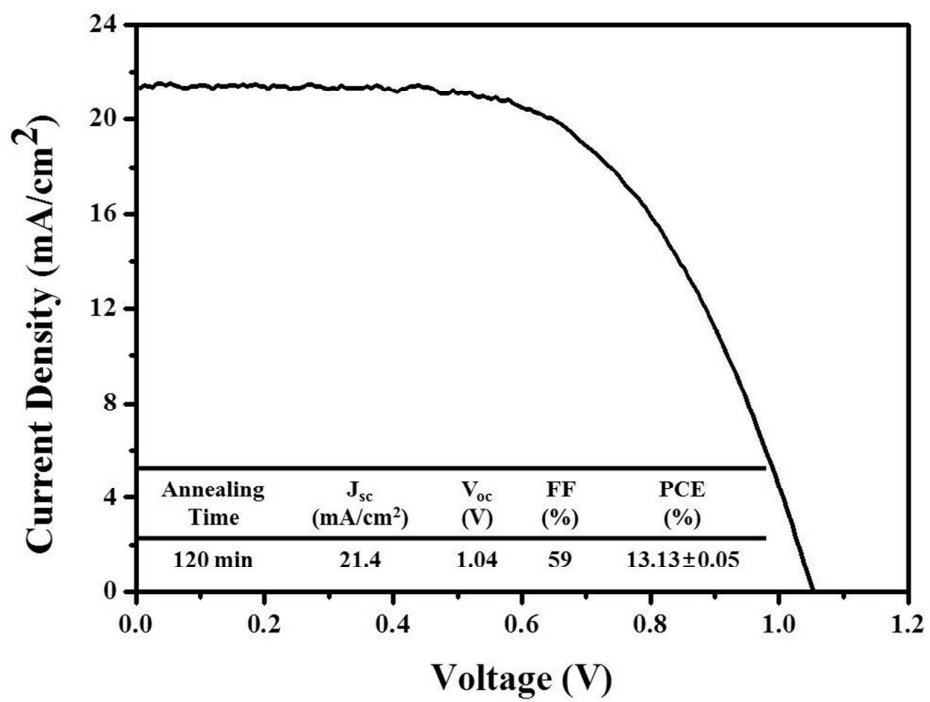


Fig. 3

*Y. J. Kim et. al*

**Fig. 4***Y. J. Kim et. al*

**Fig. 5***Y. J. Kim et. al*

**Fig. 6***Y. J. Kim et. al*

**Table 1** The photovoltaic performances of the samples annealed at each layer. The perovskite dyes were prepared using single-step process.

Annealed Sample	$J_{sc}$ (mAcm <sup>-2</sup> )	$V_{oc}$ (V)	$FF$ (%)	$PCE$ (%)
"1"	10.8	0.70	43	3.23 ± 0.87
"2"	6.38	0.69	40	1.76 ± 0.29
"3"	21.6	0.80	50	8.57 ± 0.26
"4"	15.7	0.62	31	3.12 ± 1.04

**Table 2** The photovoltaic properties of the perovskite cells annealed for different duration times at 100 °C. The perovskite dyes were prepared using single-step process.

Annealing Time (min)	$J_{sc}$ (mAcm <sup>-2</sup> )	$V_{oc}$ (V)	$FF$ (%)	$PCE$ (%)
5	15.3	0.74	35	4.01 ± 0.10
7	16.0	0.77	39	4.80 ± 0.33
10	21.6	0.80	50	8.57 ± 0.26
15	20.2	0.75	51	7.80 ± 0.11
20	20.1	0.68	45	6.15 ± 0.25

**Table 3** The photovoltaic properties of the solar cells as a function of annealing temperature for annealing time of 10 min. The perovskite dyes were prepared using single-step process.

Annealing Temp. (°C)	$J_{sc}$ (mAcm <sup>-2</sup> )	$V_{oc}$ (V)	$FF$ (%)	$PCE$ (%)
80	19.3	0.71	40	5.48 ± 0.12
100	21.6	0.80	50	8.57 ± 0.26
130	17.9	0.68	33	4.12 ± 0.30
150	14.1	0.51	35	2.52 ± 0.19